Supporting Information

Through-Space Charge Transfer Enabled Design of Nonlinear Optical Chromophores with Balanced Absorption and Efficiency

Arjun J.,[a] Aneesh Kumar R.,[b] Navjot Kaur,[c] Renjith Raveendran Pillai,[a,b] Rinu Jacob,[d] and Ramanathan Padmanaban[d]

[a] *Department of Physics, Government College Kasaragod, Vidyanagar, Kasaragod, Kerala, India.*
[b] *Department of Physics, University College, University of Kerala, Thiruvananthapuram, Kerala, India*
[c] *Department of Chemistry, Faculty of Applied and Basic Sciences, SGT University, Gurugram, 122505, Haryana, India*
[d] *Department of Chemistry, School of Physical Chemical and Applied Sciences, Pondicherry University, Puducherry, 605014, India*

*Corresponding author- Renjith Raveendran Pillai (*renjithkadavoor@gmail.com*, *drrenjith@gck.ac.in*
Phone: +918281560152)

This Supporting Information includes:

- **Table S1.** Dihedral angles (θd, θa) of DMA-Nap-TRZ in gas and solvent phases.
- **Table S2.** D, S_r, and t indices for first five excited states in DMSO.
- **Table S3.** D, S_r, and t indices for first five excited states in toluene.
- **Table S4.** Enhancement in HRS hyperpolarizability on TRZ substitution.
- **Table S5.** Enhancement in second-order hyperpolarizability on TRZ substitution.
- **Table S6.** Photophysical properties of the molecules in toluene solvent.
- **Figure S1.** NTOs (S_1-S_5) of DMA-Nap-TRZ in DMSO.
- **Figure S2.** NTOs (S_1-S_5) of DMA-AzoNap in DMSO.
- **Figure S3.** NTOs (S_1-S_5) of DMA-AzoNap-TRZ in DMSO.
- **Figure S4.** Excited state energy levels of the designed molecules.
- **Figure S5.** IGMH isosurfaces of DMA-Nap-TRZ and DMA-AzoNap-TRZ.
- **Figure S6.** CT and LE contributions for the excited states of DMA-Nap-TRZ in toluene.
- **Figure S7.** CT and LE contributions for the excited states of DMA-AzoNap in toluene.
- **Figure S8.** CT and LE contributions for the excited states of DMA-AzoNap-TRZ in toluene.
- **Figure S9.** TSCT and TBCT contributions for excited states of DMA-Nap-TRZ in toluene.
- **Figure S10.** TSCT and TBCT contributions for excited states of DMA-Nap-TRZ in DMSO.
- **Figure S11.** HRS intensity vs polarization angle (Ψ) for DMA-AzoNap at 1064 and 1340 nm in various solvents.

- **Figure S12.** HRS intensity vs polarization angle (Ψ) for DMA-AzoNap-TRZ at 1064 and 1340 nm in various solvents.
- **Figure S13.** Absorption spectra of the molecules in toluene solvent.
- **Figure S14.** FMOs of DMA, Nap, and TRZ.
- **Section S1.** Additional computational details
- **Section S2.** Frontier Molecular Orbitals (FMOs) of DMA, Nap, and TRZ

Table S1. Dihedral angles between the donor and acceptor groups and the naphthalene bridge (θ_d and θ_a) for DMA-Nap-TRZ in gas and solvent phases.

Phase	**θ_d**	**θ_a**
Gas	89.74^0	89.67^0
DMSO	89.74^0	89.72^0
Toluene	89.84^0	89.8^0
Δ^b	0.1^0	0.13^0

[b] Differences between maximum and minimum values for each θ.

Table S2. Hole-particle centroid distance (*D*), overlap (S_r), and separation (*t*) indices for the first five excited states of the studied molecules in DMSO solvent.

Molecules	**Excited states**	***D* (Å)**	**S_r (au)**	***t* (Å)**
DMA-Nap-TRZ	S_1	2.978	0.249	1.888
	S_2	2.919	0.330	1.840
	S_3	3.380	0.211	1.986
	S_4	0.718	0.721	-1.561
	S_5	0.249	0.555	-0.837
DMA-AzoNap	S_1	0.074	0.620	-1.269
	S_2	0.766	0.765	-2.349
	S_3	4.735	0.202	2.686
	S_4	0.831	0.756	-0.687
DMA-AzoNap-TRZ	S_1	0.057	0.611	-1.197
	S_2	0.805	0.768	-2.375
	S_3	4.414	0.229	2.277
	S_4	2.784	0.254	1.581
	S_5	2.909	0.334	1.761

Table S3. Hole-particle centroid distance (D), overlap (S_r), and separation (t) indices for the first five excited states of the studied molecules in toluene solvent.

Molecules	Excited states	D (Å)	S_r (au)	t (Å)
DMA-Nap-TRZ	S_1	2.978	0.249	1.888
	S_2	2.919	0.330	1.840
	S_3	3.380	0.211	1.986
	S_4	0.718	0.721	-1.561
	S_5	0.249	0.555	-0.837
DMA-AzoNap	S_1	0.069	0.618	-1.240
	S_2	0.069	0.618	-1.240
	S_3	4.561	0.262	2.235
	S_4	0.838	0.753	-0.710
DMA-AzoNap-TRZ	S_1	0.054	0.609	-1.174
	S_2	0.273	0.740	-3.063
	S_3	3.699	0.420	0.736
	S_4	2.824	0.2542	1.624
	S_5	2.911	0.333	1.761

Table S4. $\beta_{HRS}(\times 10^{-30} esu)$ for DMA-AzoNap and DMA-AzoNap-TRZ at 1064 and 1340 nm in various solvents. The percent change indicates the enhancement in HRS intensity upon TRZ substitution.

Solvent		DMA-AzoNap	DMA-AzoNap-TRZ	Percent change (%)
DMSO	β_{HRS}^{1064}	76.48	85.83	10.9
	β_{HRS}^{1340}	52.52	57.59	8.8
Ethanol	β_{HRS}^{1064}	72.25	81.61	11.5
	β_{HRS}^{1340}	49.91	55.11	9.4
THF	β_{HRS}^{1064}	70.68	79.07	10.6
	β_{HRS}^{1340}	49.02	53.62	8.6
Toluene	β_{HRS}^{1064}	65.73	71.9	8.6
	β_{HRS}^{1340}	46.1	49.35	6.6
Gas	β_{HRS}^{1064}	34.85	37.28	6.5
	β_{HRS}^{1340}	26.14	27.51	5.0

Table S5. $\gamma(\times 10^{-36} esu)$ for DMA-AzoNap and DMA-AzoNap-TRZ at 1064 and 1340 nm in various solvents. The percent change indicates the enhancement in HRS intensity upon TRZ substitution.

Solvent		DMA-AzoNap	DMA-AzoNap-TRZ	Percent change (%)
DMSO	$\gamma^{1064}(\omega)$	444.94	553.45	19.6
	$\gamma^{1064}(2\omega)$	867.97	1102.95	21.3
	$\gamma^{1340}(\omega)$	396.72	493.13	19.6
	$\gamma^{1340}(2\omega)$	528.01	667.81	20.9
Toluene	$\gamma^{1064}(\omega)$	343.82	436.15	21.2
	$\gamma^{1064}(2\omega)$	742.59	948.22	21.7
	$\gamma^{1340}(\omega)$	307.71	389.9	21.1
	$\gamma^{1340}(2\omega)$	461.69	588.17	21.5

Table S6. Photophysical properties and excited state characteristics of the designed molecules in toluene solvent at CAM-B3LYP/6-311G(d) level of theory.

	Excited States	Wavelength (nm)	Osc. Strength (f)	Energy (eV)	Transition Type
DMA-Nap-TRZ	S_1	356.04	0.0002	3.4823	TSCT
	S_2	324.45	0.0429	3.8213	TSCT
	S_3	321.56	0.0001	3.8557	TBCT
	S_4	275.89	0.1333	4.494	HLCT
	S_5	275.12	0.0119	4.5065	HLCT
DMA-AzoNap	S_1	445.82	0.0255	2.7811	LE
	S_2	373.68	1.1448	3.3179	LE
	S_3	370.41	0.0376	3.3472	TBCT
	S_4	290.20	0.0308	4.2724	LE
DMA-AzoNap-TRZ	S_1	447.81	0.0137	2.7687	LE
	S_2	378.30	1.1086	3.2774	LE
	S_3	377.09	0.2056	3.2879	TBCT
	S_4	352.90	0.0001	3.5133	TSCT
	S_5	320.71	0.0412	3.8659	TSCT

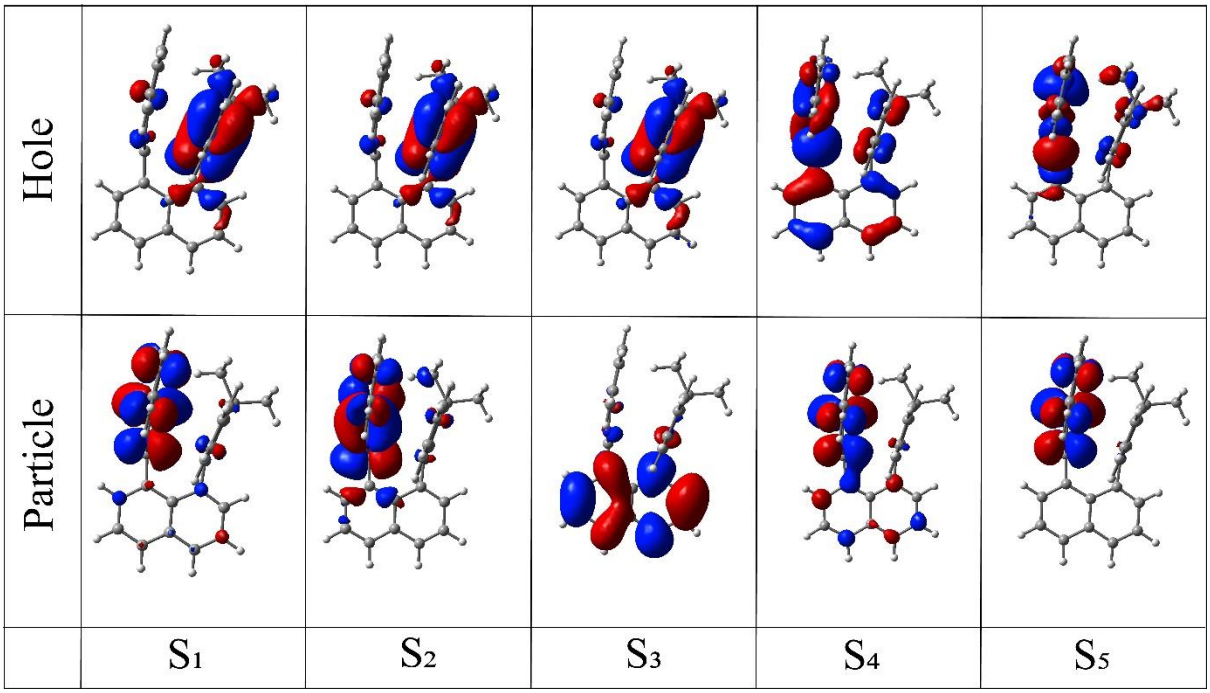

Figure S1. Natural Transition Orbitals (NTOs) for the first five excited states (S_1 - S_5) of DMA-Nap-TRZ in DMSO solvent.

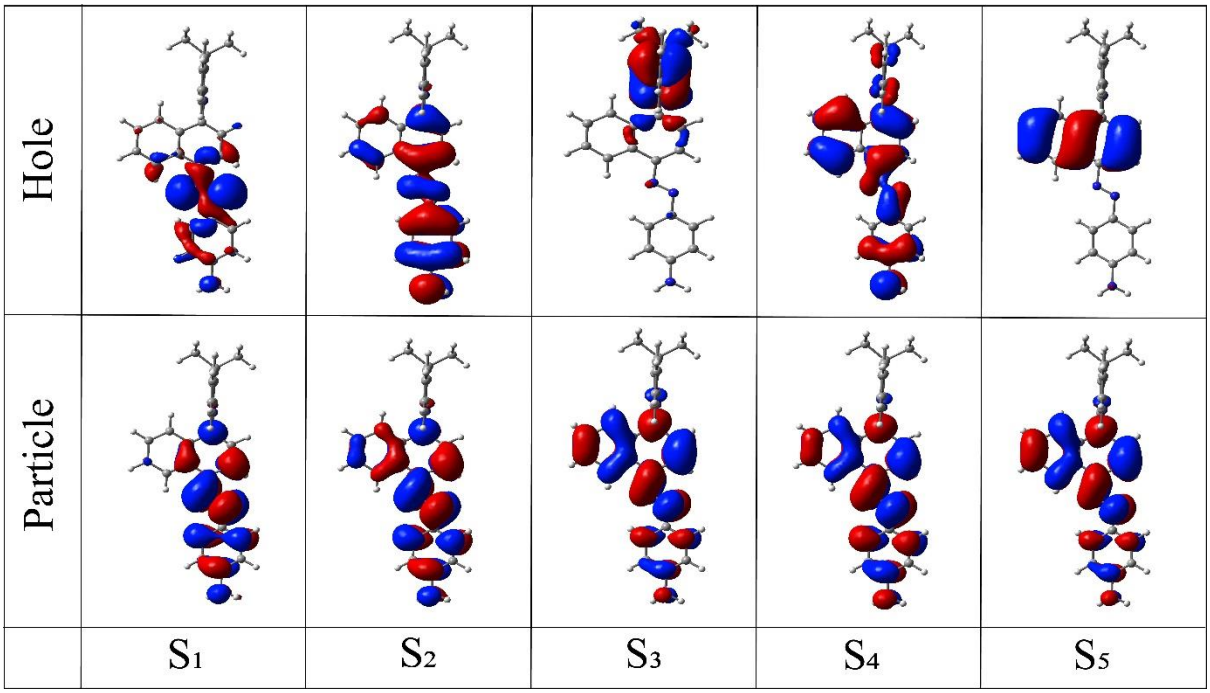

Figure S2. Natural Transition Orbitals (NTOs) for the first five excited states (S_1 - S_5) of DMA-AzoNap in DMSO solvent.

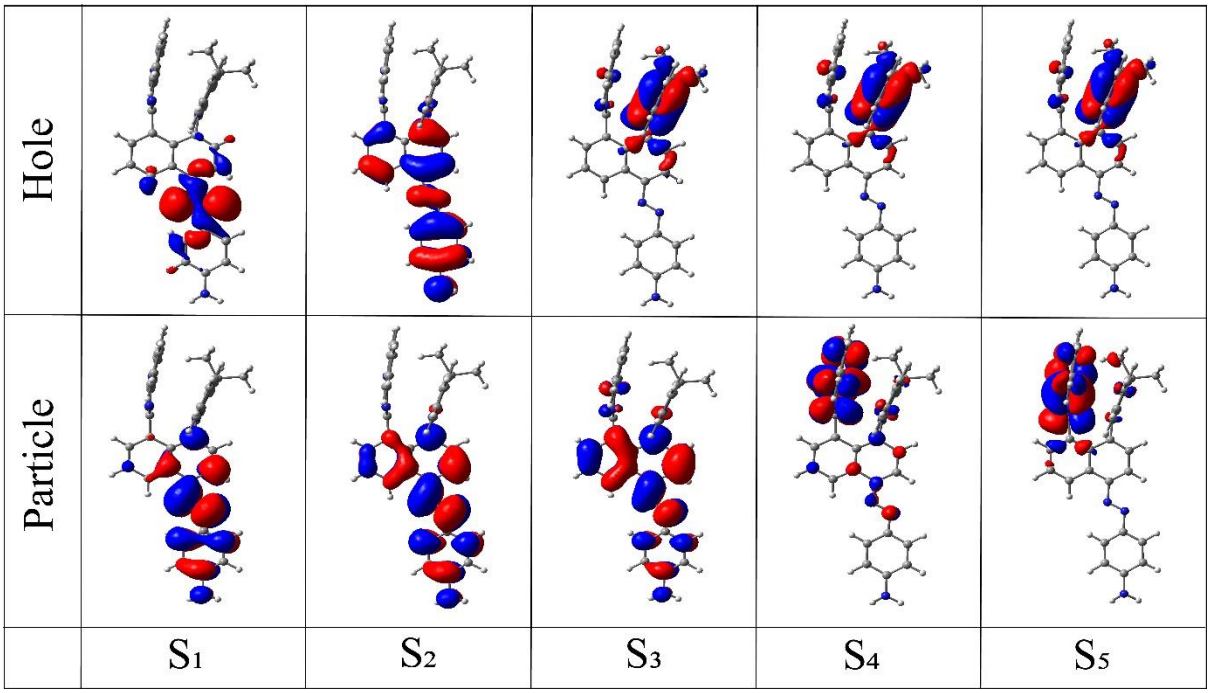

Figure S3. Natural Transition Orbitals (NTOs) for the first five excited states (S_1 - S_5) of DMA-AzoNap-TRZ in DMSO solvent.

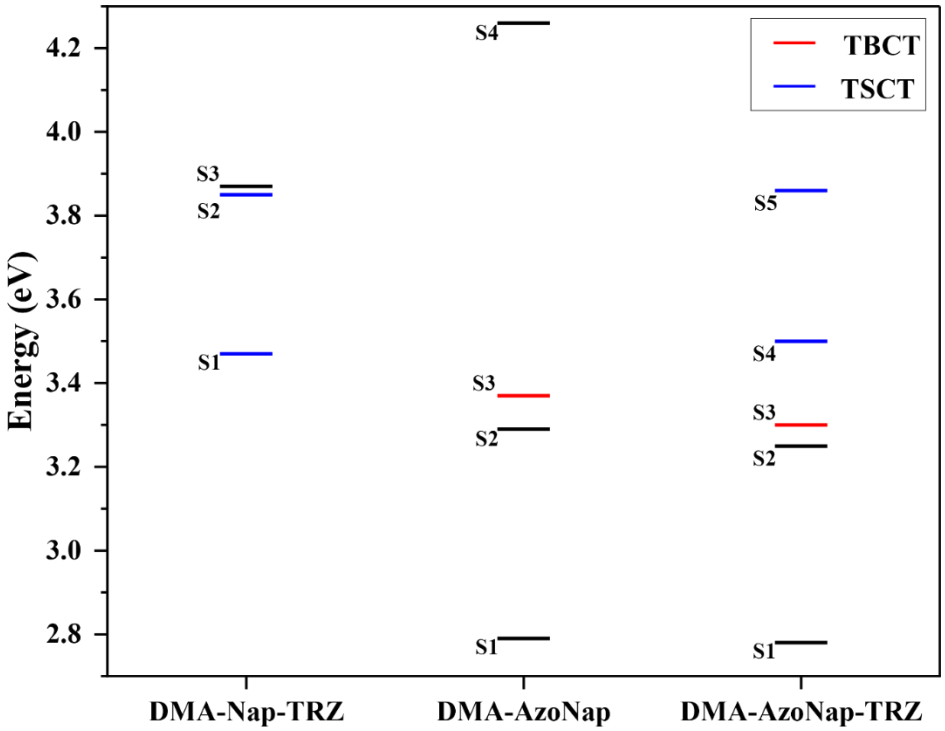

Figure S4. Excited state energy levels of the designed molecules.

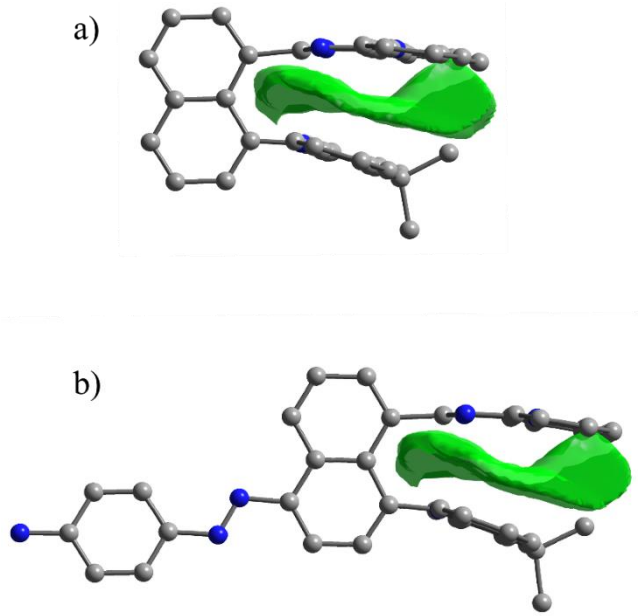

Figure S5. The IGMH isosurfaces for molecules a) DMA-Nap-TRZ, and b) DMA-AzoNap-TRZ.

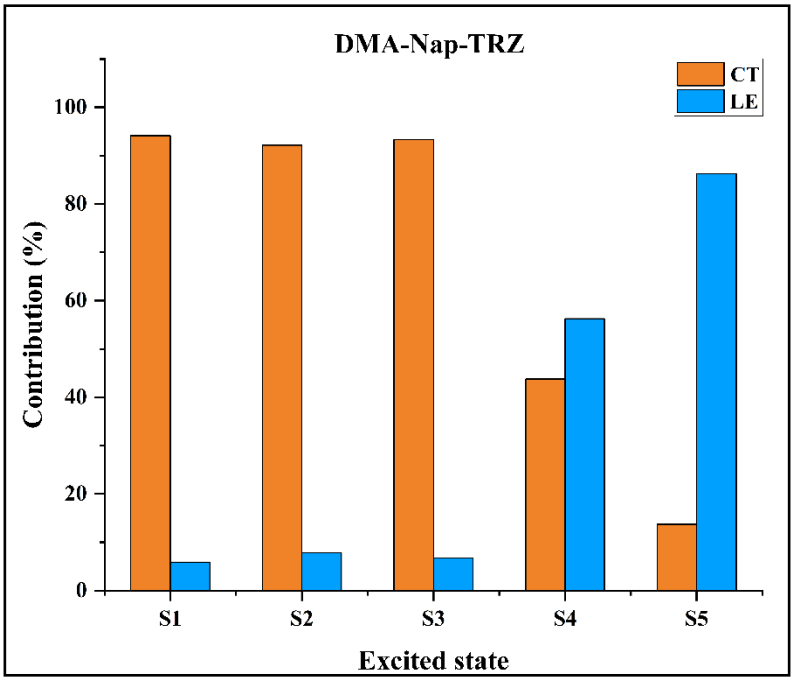

Figure S6. Percentage contributions of charge-transfer (CT) and local-excitation (LE) character for the excited states of DMA-Nap-TRZ in toluene solvent.

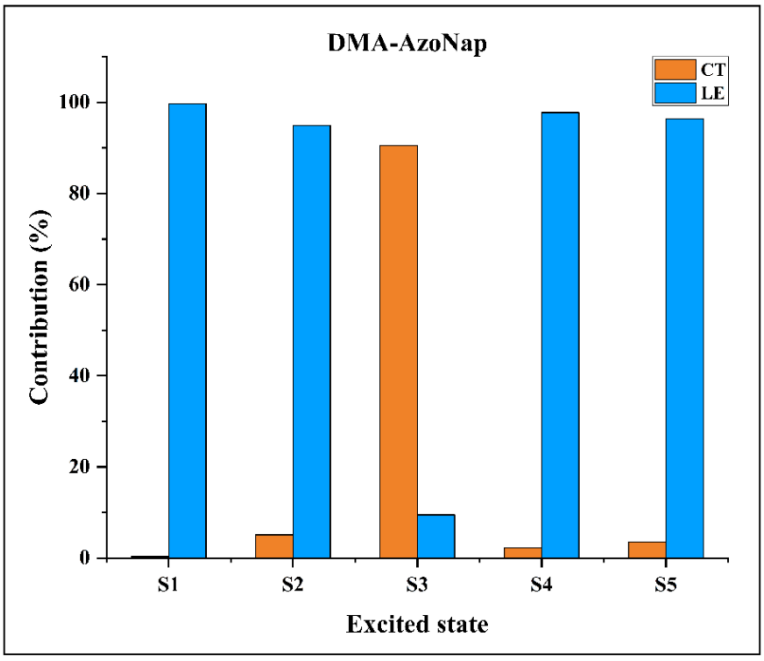

Figure S7. Percentage contributions of charge-transfer (CT) and local-excitation (LE) character for the excited states of DMA-AzoNap in toluene solvent.

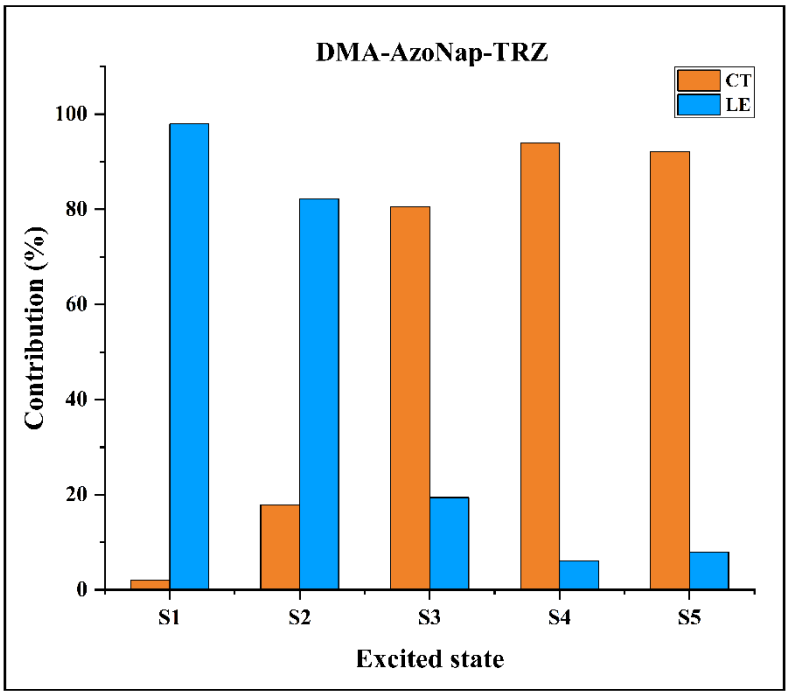

Figure S8. Percentage contributions of charge-transfer (CT) and local-excitation (LE) character for the excited states of DMA-AzoNap-TRZ in toluene solvent.

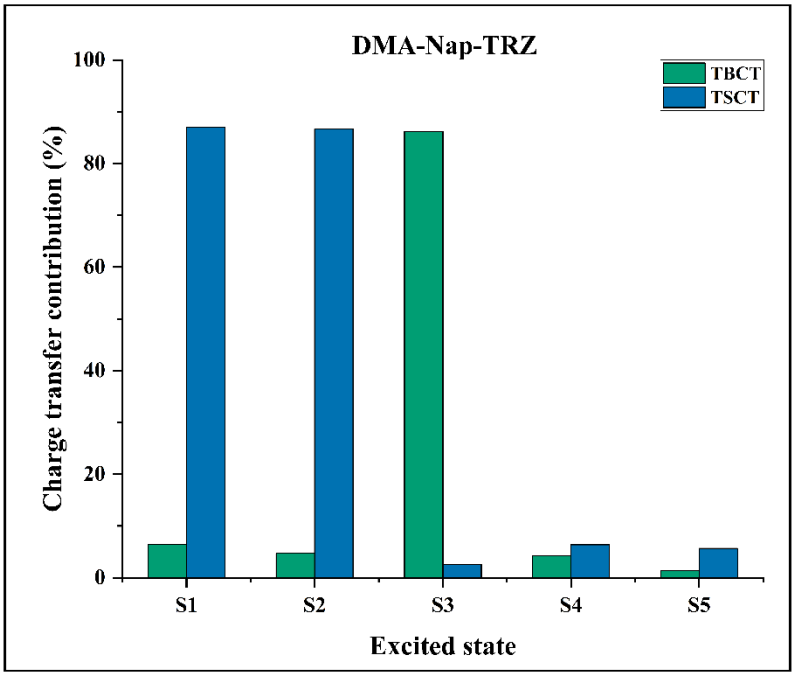

Figure S9. Percentage contributions of Through-Space Charge Transfer (TSCT) and Through-Bond Charge Transfer (TBCT) character for the excited states of DMA-Nap-TRZ in toluene solvent.

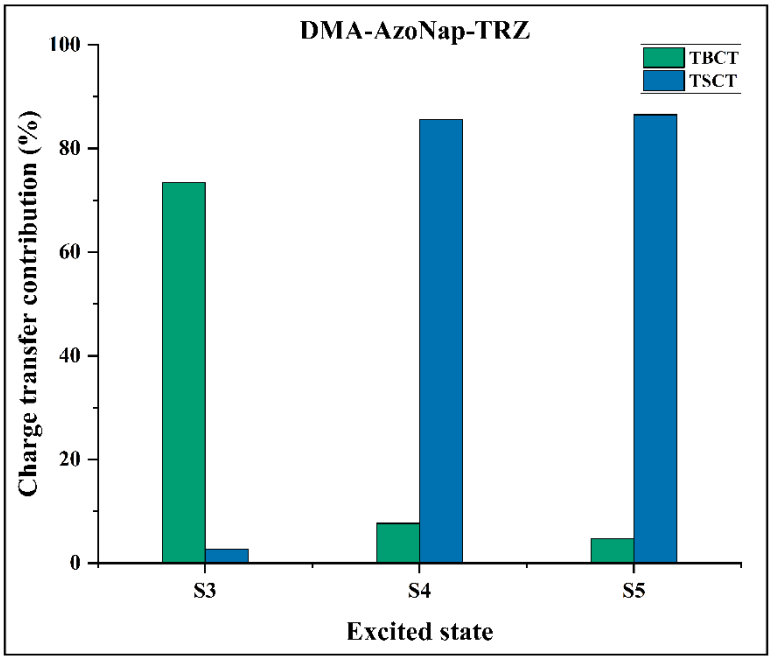

Figure S10. Percentage contributions of Through-Space Charge Transfer (TSCT) and Through-Bond Charge Transfer (TBCT) character for the excited states of DMA-AzoNap-TRZ in toluene solvent.

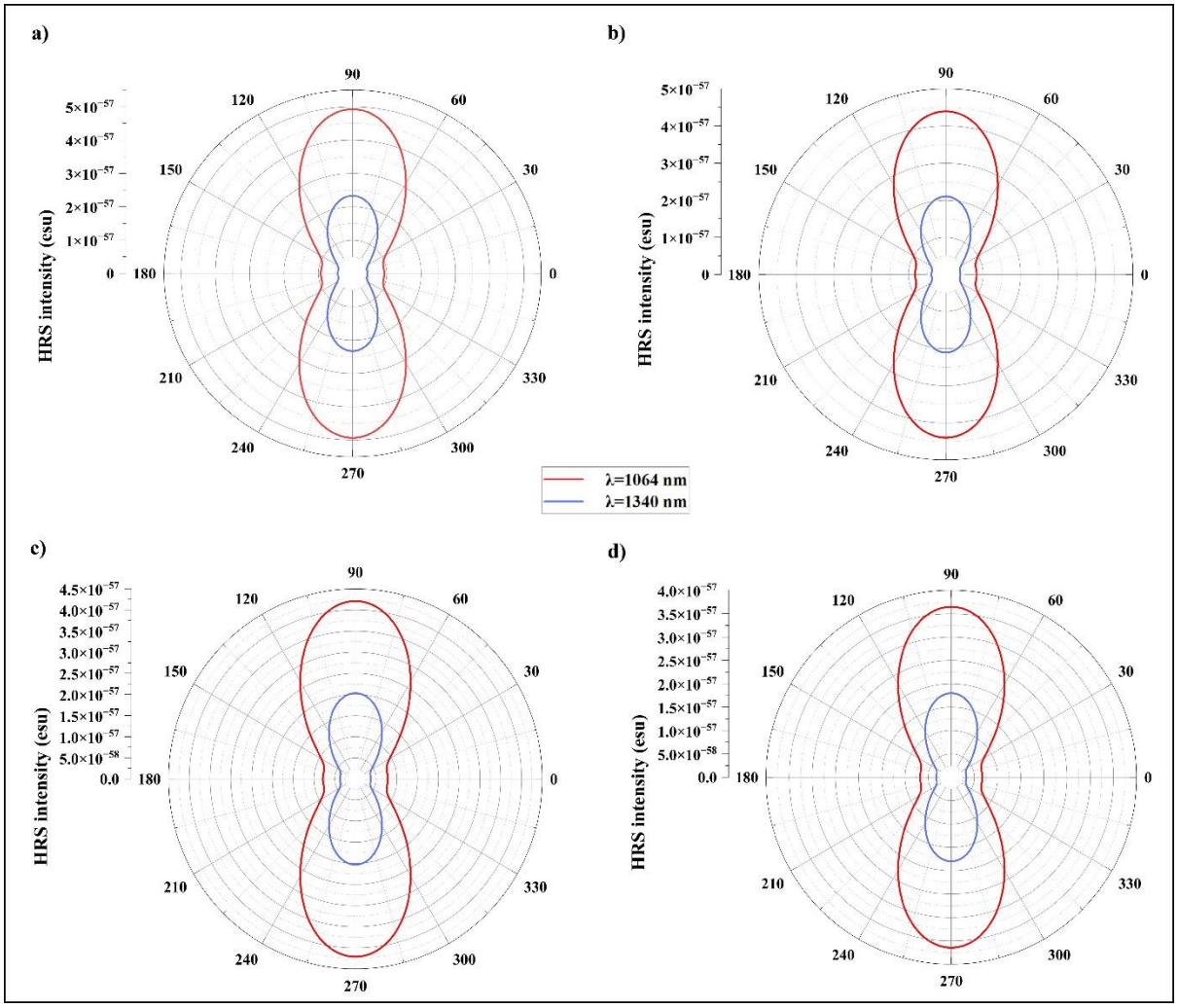

Figure S11. Variation of hyper-Rayleigh scattering (HRS) intensity with polarization angle (Ψ) for DMA-AzoNap at excitation wavelengths of 1064 and 1340 nm in (a) DMSO, (b) ethanol, (c) THF, and (d) toluene.

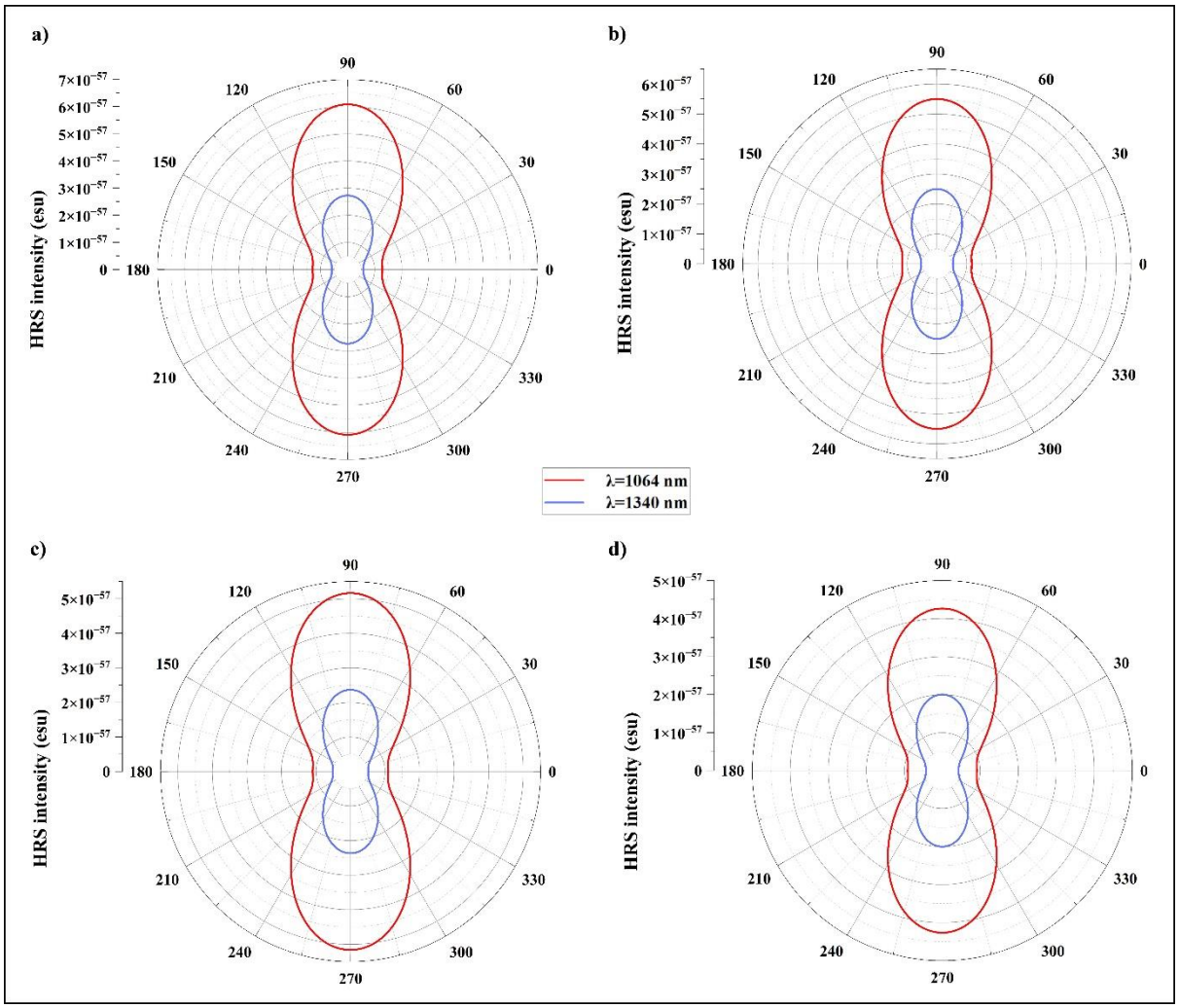

Figure S12. Variation of hyper-Rayleigh scattering (HRS) intensity with polarization angle (Ψ) for DMA-AzoNap-TRZ at excitation wavelengths of 1064 and 1340 nm in (a) DMSO, (b) ethanol, (c) THF, and (d) toluene.

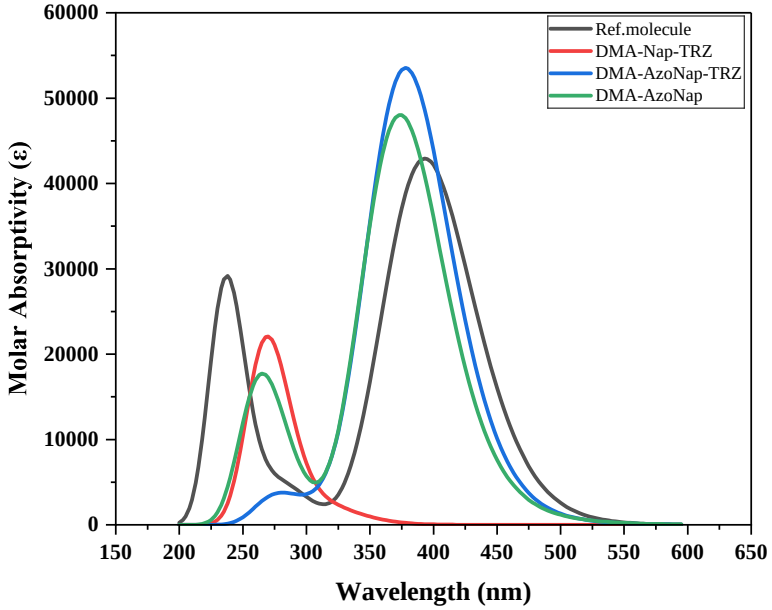

Figure S13: Calculated absorption spectra for the designed molecules in toluene solvent at CAM-B3LYP/6-311G(d) level of theory.

Section S1. Additional Computational Details

All quantum chemical calculations were carried out using the Gaussian 16 software package.[1] The M06-2X density functional was employed in combination with the 6-311G(d) basis set for geometry computations.[2] The UltraFine integration grid (a pruned grid consisting of 99 radial shells and 590 angular points per atom) was used for the numerical evaluation of the DFT integrals.
Full geometry optimizations were performed without any symmetry constraints, and the nature of each stationary point was verified through frequency calculations to ensure the absence of imaginary frequencies. Geometry convergence was achieved when all of the following criteria were satisfied simultaneously:

- Maximum force: $<$ 0.00045 Hartree/Bohr
- Root-mean-square (RMS) force: $<$ 0.0003 Hartree/Bohr
- Maximum displacement: $<$ 0.0018 Bohr
- RMS displacement: $<$ 0.0012 Bohr

The self-consistent field (SCF) procedure was considered converged when the change in total electronic energy between successive cycles was less than 10^{-8} Hartree, which corresponds to the default convergence threshold in Gaussian 16.
The $\langle\beta_{HRS}\rangle$ can be expressed in terms of $\langle\beta^2_{ZZZ}\rangle$ and $\langle\beta^2_{ZXX}\rangle$. The corresponding relations are given below, where symmetry conditions are neglected.[3–5]

$$\begin{aligned}\langle\beta^2_{ZZZ}\rangle =& \frac{1}{7}\sum_{\zeta}^{x,y,z}\beta^2_{\zeta\zeta\zeta} + \frac{4}{35}\sum_{\zeta\neq\eta}^{x,y,z}\beta^2_{\zeta\zeta\eta} + \frac{2}{35}\sum_{\zeta\neq\eta}^{x,y,z}\beta_{\zeta\zeta\zeta}\beta_{\zeta\eta\eta} + \frac{4}{35}\sum_{\zeta\neq\eta}^{x,y,z}\beta_{\eta\zeta\zeta}\beta_{\zeta\zeta\eta} \\ &+ \frac{4}{35}\sum_{\zeta\neq\eta}^{x,y,z}\beta_{\zeta\zeta\zeta}\beta_{\eta\eta\zeta} + \frac{1}{35}\sum_{\zeta\neq\eta}^{x,y,z}\beta^2_{\eta\zeta\zeta} + \frac{4}{105}\sum_{\zeta\neq\eta\neq\xi}^{x,y,z}\beta_{\zeta\zeta\eta}\beta_{\eta\xi\xi} \\ &+ \frac{1}{105}\sum_{\zeta\neq\eta\neq\xi}^{x,y,z}\beta_{\eta\zeta\zeta}\beta_{\eta\xi\xi} + \frac{4}{105}\sum_{\zeta\neq\eta\neq\xi}^{x,y,z}\beta_{\zeta\zeta\eta}\beta_{\xi\xi\eta} + \frac{2}{210}\sum_{\zeta\neq\eta\neq\xi}^{x,y,z}\beta^2_{\zeta\eta\xi} \\ &+ \frac{4}{105}\sum_{\zeta\neq\eta\neq\xi}^{x,y,z}\beta_{\zeta\eta\xi}\beta_{\eta\xi\xi}\end{aligned} \tag{S1}$$

$$\begin{aligned}\langle\beta_{ZXX}^2\rangle =& \frac{1}{35}\sum_{\zeta}^{x,y,z}\beta_{\zeta\zeta\zeta}^2 + \frac{4}{105}\sum_{\zeta\neq\eta}^{x,y,z}\beta_{\zeta\zeta\zeta}\beta_{\zeta\eta\eta} - \frac{2}{35}\sum_{\zeta\neq\eta}^{x,y,z}\beta_{\zeta\zeta\zeta}\beta_{\eta\eta\zeta} + \frac{8}{105}\sum_{\zeta\neq\eta}^{x,y,z}\beta_{\zeta\zeta\eta}^2 \\ &+ \frac{3}{35}\sum_{\zeta\neq\eta}^{x,y,z}\beta_{\zeta\eta\eta}^2 - \frac{2}{35}\sum_{\zeta\neq\eta}^{x,y,z}\beta_{\zeta\zeta\eta}\beta_{\eta\zeta\zeta} + \frac{1}{35}\sum_{\zeta\neq\eta\neq\xi}^{x,y,z}\beta_{\zeta\eta\eta}\beta_{\zeta\xi\xi} \\ &- \frac{2}{105}\sum_{\zeta\neq\eta\neq\xi}^{x,y,z}\beta_{\zeta\zeta\xi}\beta_{\eta\eta\xi} - \frac{2}{105}\sum_{\zeta\neq\eta\neq\xi}^{x,y,z}\beta_{\zeta\zeta\eta}\beta_{\eta\xi\xi} + \frac{2}{35}\sum_{\zeta\neq\eta\neq\xi}^{x,y,z}\beta_{\zeta\eta\xi}^2 \\ &- \frac{2}{105}\sum_{\zeta\neq\eta\neq\xi}^{x,y,z}\beta_{\zeta\eta\xi}\beta_{\eta\zeta\xi}\end{aligned} \tag{S2}$$

where *ZZZ* and *ZXX* refer to the laboratory coordinate system, and x, y, and z correspond to the molecular coordinates. The indices ζ, η, and ξ represent the molecular frame Cartesian axes x, y, and z, respectively.

Section S2. Frontier Molecular Orbitals (FMOs) of DMA, Nap, and TRZ

The molecular π-bridge is a decisive factor that actively governs the intramolecular charge transfer (ICT) and resulting nonlinear optical (NLO) properties, serving as far more than a passive spacer. For efficient, long-range charge transfer to occur, the FMOs of the bridge must be appropriately matched with those of the donor (D) and acceptor (A). The optimal design requires the bridge's HOMO and LUMO energy levels to lie energetically between their counterparts in the donor and acceptor, following the specific order $E_D^H \geq E_\pi^H \gg E_A^H$ and $E_D^L \gg E_\pi^L \geq E_A^L$. This specific alignment allows the bridge's orbitals to have appropriate involvement by mixing with the donor and acceptor orbitals to form the overall FMOs of the complete D-π-A system. The bridge's specific composition, conjugation length, and orientation are all critical factors that modulate these electronic properties.[6] Applying this principle, FMO analysis of the individual DMA, Nap, and TRZ fragments confirmed that our system meets this key requirement. As depicted in the FMO diagram (Figure S14), the HOMO and LUMO energy levels of the Nap bridge are ideally situated between those of the DMA donor and the TRZ acceptor, providing an optimal energetic pathway for efficient intramolecular charge transfer.

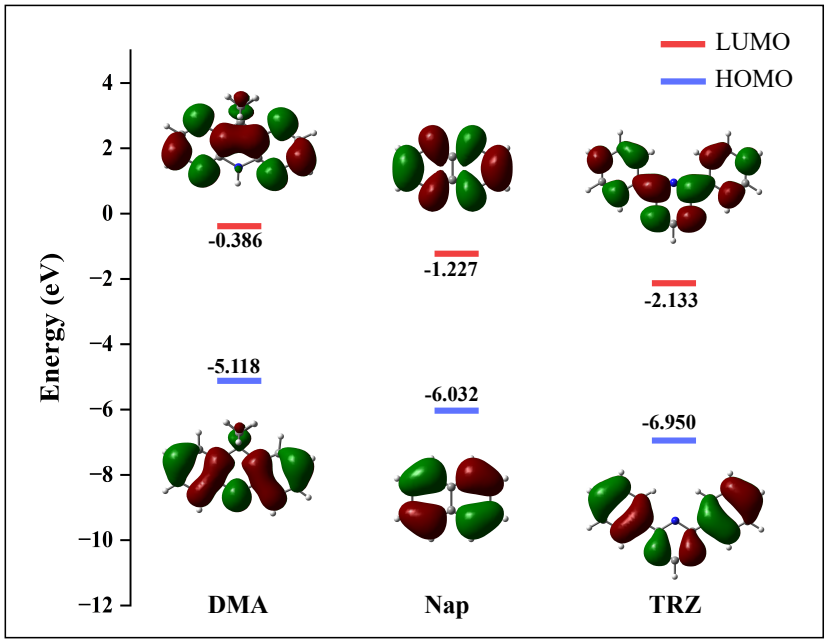

Figure S14: FMOs of the DMA, Nap and TRZ calculated at B3LYP/6-311G(d) level of theory.

References

[1] M. J. Frisch, G. W. Trucks, H. B. Schlegel, G. E. Scuseria, M. A. Robb, J. R. Cheeseman, G. Scalmani, V. Barone, G. A. Petersson, H. Nakatsuji, X. Li, M. Caricato, A. V. Marenich, J. Bloino, B. G. Janesko, R. Gomperts, B. Mennucci, H. P. Hratchian, J. V. Ortiz, A. F. Izmaylov, J. L. Sonnenberg, D. Williams-Young, F. Ding, F. Lipparini, F. Egidi, J. Goings, B. Peng, A. Petrone, T. Henderson, D. Ranasinghe, V. G. Zakrzewski, J. Gao, N. Rega, G. Zheng, W. Liang, M. Hada, M. Ehara, K. Toyota, R. Fukuda, J. Hasegawa, M. Ishida, T. Nakajima, Y. Honda, O. Kitao, H. Nakai, T. Vreven, K. Throssell, J. A. Montgomery, Jr., J. E. Peralta, F. Ogliaro, M. J. Bearpark, J. J. Heyd, E. N. Brothers, K. N. Kudin, V. N. Staroverov, T. A. Keith, R. Kobayashi, J. Normand, K. Raghavachari, A. P. Rendell, J. C. Burant, S. S. Iyengar, J. Tomasi, M. Cossi, J. M. Millam, M. Klene, C. Adamo, R. Cammi, J. W. Ochterski, R. L. Martin, K. Morokuma, O. Farkas, J. B. Foresman and D. J. Fox, *Gaussian˜16 Revision C.01*, 2016, Gaussian Inc. Wallingford CT.

[2] Y. Zhao and D. G. Truhlar, *Accounts of chemical research*, 2008, **41**, 157–167.

[3] L. M. Abegao, R. D. Fonseca, F. A. Santos, J. J. Rodrigues, K. Kamada, C. R. Mendonça, S. Piguel and L. De Boni, *RSC advances*, 2019, **9**, 26476–26482.

[4] F. A. Santos, C. E. Cardoso, J. J. Rodrigues Jr, L. De Boni and L. M. Abegão, Photonics, 2023, p. 545.

[5] E. Bogdan, A. Plaquet, L. Antonov, V. Rodriguez, L. Ducasse, B. Champagne and F. Castet, *The Journal of Physical Chemistry C*, 2010, **114**, 12760–12768.

[6] C.-C. Yang, X. Su, Q.-Z. Zheng, J. Chen, W. Q. Tian, W.-Q. Li and L. Yang, *Physical Chemistry Chemical Physics*, 2023, **25**, 31481–31492.